International Journal of Pharmaceutics 429 (2012) 69–77

Contents lists available at SciVerse ScienceDirect

International Journal of Pharmaceutics

journal homepage: www.elsevier.com/locate/ijpharm

Polymorphic form of piroxicam influences the performance of amorphous material prepared by ball-milling

Kaisa Naelapää [a,*], Johan Peter Boetker [a], Peep Veski [b], Jukka Rantanen [a], Thomas Rades [c], Karin Kogermann [b]

[a] Department of Pharmaceutics and Analytical Chemistry, Faculty of Health and Medical Sciences, University of Copenhagen, Copenhagen, Denmark
[b] Department of Pharmacy, Faculty of Medicine, University of Tartu, Tartu, Estonia
[c] School of Pharmacy, University of Otago, Dunedin, New Zealand

ARTICLE INFO

Article history:
Received 2 December 2011
Received in revised form 26 January 2012
Accepted 6 March 2012
Available online 14 March 2012

Keywords:
Amorphous
Thermal behavior
Solid state transformations
Physical stability
Variable temperature X-ray powder diffractometry (VT-XRPD)
Raman spectroscopy
Principal component analysis (PCA)
Piroxicam polymorphs
Pair-wise distribution function (PDF)

ABSTRACT

The objective of this study was to investigate the influence of the starting solid state form of piroxicam (anhydrate form I: PRXAH I vs form II: PRXAH II) on the properties of the resulting amorphous material. The second objective was to obtain further insight into the impact of critical factors like thermal stress, dissolution medium and storage conditions on the thermal behavior, solid state transformations and physical stability of amorphous materials. For analysis differential scanning calorimetry (DSC), Raman spectroscopy and X-ray powder diffractometry (XRPD) were used. Pair-wise distribution function (PDF) analysis of the XRPD data was performed. PDF analysis indicated that the recrystallization behavior of amorphous samples was influenced by the amount of residual order in the samples. The recrystallization behavior of amorphous samples prepared from PRXAH I showed similarity to the starting material, whereas the recrystallization behavior of amorphous samples prepared from PRXAH II resembled to that of the PRX form III (PRXAH III). Multivariate data analysis (MVDA) helped to identify that the influence of storage time and temperature was more pronounced in the case of amorphous PRX prepared from PRXAH I. Furthermore, the wet slurry experiments with amorphous materials revealed the recrystallization of amorphous material as PRXMH in the biorelevant medium.

1. Introduction

In recent years the magnitude of the research emphasizing the importance of different polymorphic forms in pharmaceutical development and manufacturing has increased significantly. One of the main objectives of the Quality by Design (QbD) approach is to emphasize the need for science-based understanding of factors affecting the functionality of a given dosage form. The International Conference on Harmonization (ICH) Q8(R2) guideline on Pharmaceutical Development refers to the importance of ensuring and maintaining the specifically designed physicochemical properties of a drug substance (e.g., its solid state properties) throughout the product shelf life as well as after administration (ICH, 2009). Especially in case of an amorphous drug substance which induces a supersaturated solution in the gastrointestinal lumen and can be considered as supersaturated drug delivery system (SDDS) (Brouwers et al., 2009). The comprehensive understanding of attributes affecting the drug substance properties is pivotal, as critical material properties can be linked to the drug product processability, pharmaceutical quality (including stability) and biological performance. To fully understand the developed formulations (e.g., SDDS) and its properties, it is highly recommended to plan the investigations carefully as this will help to foresee in vivo performance (Augustijns and Brewster, 2012; Brouwers et al., 2009).

The amorphous form is a high energy form of the solid state, which may include different degrees of kinetic and structural disorder. The physical stability of amorphous materials upon storage is determined by several factors such as its energetic state, fragility, local mobility and the presence of reaction (i.e., crystallization) accelerators (e.g., impurities and moisture) (Morris et al., 2001). Understanding the impact of directly controllable factors (e.g., temperature, time) during the preparation of amorphous drug will provide information on the recrystallization behavior and can be used as a rational basis to increase the physical stability of amorphous materials (Boetker et al., 2011; Karmwar et al., 2011a,b).

Crystallization is a two-step process including nucleation and crystal growth. Nucleation, among other factors, is affected by the presence of a residual crystalline phase and seeding. Several methods, allowing prediction of the crystallization of amorphous

* Corresponding author at: Universitetsparken 2, DK-2100 Copenhagen, Denmark. Tel.: +45 30 35 61 55; fax: +45 30 36 63 00.
E-mail address: kn@farma.ku.dk (K. Naelapää).

0378-5173/$ – see front matter © 2012 Elsevier B.V. All rights reserved.
doi:10.1016/j.ijpharm.2012.03.008

active pharmaceutical ingredients (APIs) based on their relaxation behavior, have been proposed (Craig et al., 2000; Graeser et al., 2009; Hilden and Morris, 2003). In addition, changes in the physical properties of amorphous material upon preparation, such as its density, viscosity, heat capacity, and diffusion behavior (Boetker et al., 2011), enable the investigation of the recrystallization behavior of amorphous systems and to draw conclusions relating to their stability (Surana et al., 2004a,b). The physical stability of amorphous APIs has previously been studied using various storage conditions, mainly at different temperatures, with an emphasis on relaxation of the amorphous form (Karmwar et al., 2011a), at different relative humidities (Graeser et al., 2009), and in the presence of various excipients (e.g., polymers) (Aso et al., 2003; Hilden and Morris, 2003; Ingkatawornwong et al., 2001; Shibata et al., 2006).

The physical stability of amorphous materials can be influenced by the preparation method (Savolainen et al., 2007; Surana et al., 2004b), thermal history (Surana et al., 2004a), and starting crystalline form when milling is used as the preparation method (Crowley and Zografi, 2002). However, it is not yet clear if the differences in the physical stability are derived from the existence of several "amorphous states" (Winkel et al., 2007) or if the starting crystalline form of an API produces amorphous forms that differ in stability as a consequence of different degrees of molecule disorder, but do not constitute different states in a thermodynamic sense (Graeser et al., 2009). The local order of an amorphous form can be studied, for example by applying atomic pair-wise distribution function (PDF) analysis directly to X-ray diffraction patterns. The PDF trace displays the probability of finding atoms separated by a distance (r). The PDF hence assesses the inter-atomic distances of the material (Bates et al., 2006; Dinnebier and Billinge, 2008).

Piroxicam (PRX) is a non-steroidal anti-inflammatory drug that has been extensively used as a model compound in studies where the aims have been to enhance solubility, characterize the solid state and investigate process induced changes, due to its poor aqueous solubility (Jinno et al., 2000), polymorphic behavior (Bordner et al, 1984; Kojic-Prodic and Ruzic-Toros, 1982; Sheth et al., 2004b; Vrečer et al., 2003), and solid state transformations (Kogermann et al., 2007a,b, 2008, 2011; Shakhtshneider et al., 2007). PRX can exist in three crystalline anhydrous forms (PRXAH), however the crystalline structure of PRXAH III is not referenced in the Cambridge Structural Database (CSD). As reported previously (Kogermann et al., 2011; Sheth et al., 2004a), PRXAH I and II crystalline forms can be transformed to amorphous PRX during ball-milling for 180 min at low temperature (as determined by the presence of only a halo in the X-ray powder diffractograms). Investigation of the three dimensional structures of PRXAH I and II show that they have relatively similar packing motifs and only small differences in hydrogen bonding separate these two solid forms (Kojic-Prodic and Ruzic-Toros, 1982; Reck et al., 1988; Vrečer et al., 2003). It has been reported that amorphous PRX forms, prepared by cryomilling of PRXAH I or II have a similar short range order determined by PDF calculations, but different crystallization behavior during heating (Sheth et al., 2004b).

This study aims to provide a practical insight into the influence of polymorphic form of PRX on the performance of amorphous material prepared by ball-milling. The impact of several critical factors on the stability of amorphous PRX prepared by ball-milling of anhydrous PRX I and II at low temperature for 180 min were investigated. First, PDF analysis was employed to identify differences in the amorphous samples prepared from the different starting polymorphs. Secondly, the effect of temperature, during non-isothermal heating as well as during storage of amorphous material, on recrystallization was investigated by using X-ray powder diffractometry (XRPD), Raman spectroscopy, and differential scanning calorimetry (DSC). Furthermore, the stability of amorphous PRX was studied in the presence of biorelevant dissolution medium during dissolution testing and subsequent solid state changes were monitored with in-line Raman spectroscopy. MVDA tools were applied for data analysis.

2. Materials and methods

2.1. Materials

The model compound, PRX (USP grade, 99.44%), was obtained from Letco Medical Inc. (AL, USA) as anhydrous PRX form I (PRXAH I). Anhydrous PRX form II (PRXAH II) was crystallized from a hot methanol solution and dried at room temperature (Vrečer et al., 2003). Anhydrous PRX form III (PRXAH III) was prepared according to Vrečer et al. (2003) by spray-drying PRXAH I from absolute ethanol. Identification and characterization of all forms of PRX was based on XRPD, Raman spectroscopy, DSC, and high performance liquid chromatography (HPLC).

PRX monohydrate (PRXMH) was prepared by crystallization from hot aqueous solution (Kogermann et al., 2007a). Chemically pure amorphous PRX, confirmed by HPLC, was obtained by ball-milling of PRXAH I and II at low temperature for 180 min (Kogermann et al., 2011).

2.2. Methods

2.2.1. X-ray powder diffractometry (XRPD)

XRPD analysis was performed using an X'Pert PRO MPD X-ray diffractometer (PANalytical B.V., Almelo, The Netherlands) and Ni filtered Cu Kα_1 radiation (λ = 1.541 Å). Samples were measured in Bragg Brentano reflection mode in the range of 2–40° 2θ using a PIXel detector (PANalytical B.V., Almelo, The Netherlands) and a step size of 0.0334° 2θ. The operating current and voltage were 40 mA and 45 kV, respectively. Data were collected using X'Pert Data Collector (PANalytical B.V., Almelo, The Netherlands). Experimental results were compared to the theoretical patterns in the Cambridge Structural Database (CSD, Cambridge, UK) (Allen, 2002). Refcodes BIYSEH (Kojic-Prodic and Ruzic-Toros, 1982) and BIYSEH02 (Reck et al., 1988) were used as reference crystal structures, for PRXAH I and II, respectively. For identification of PRXAH III the X-ray powder diffractogram published by Vrečer et al. (2003) was used, with the unique peak allocations appearing at 9.1°, 13.1°, 18.2°, 28.4° and 29.5° 2θ.

For non-isothermal (variable temperature) XRPD (VT-XRPD) measurements an Anton Paar CHC chamber (Anton Paar GmbH, Graz, Austria) was mounted on the goniometer of the diffractometer. A 0.2 mm deep sample holder was used. VT-XRPD scans were obtained from 30 to 160 °C at 10 °C intervals. The heating rate of 10 K/min was controlled by TCU 110 temperature controller (Anton Paar GmbH) and the samples were equilibrated for 60 s before initiating the scan.

2.2.2. Raman spectroscopy

Raman spectra were collected using a Raman spectrometer (Control Development Inc., South Bend, IN, USA) equipped with a T.E. cooled FFT-CCD detector (1024 × 64) and a two fiber coaxial optic probe. The laser source was a 300 mW diode laser system operating at 785 nm (Control Development, Inc., South Bend, IN, USA). The detection range was from 500 to 2200 cm^{-1}. A total of 8 scans per spectrum with a 1.0 s integration time were acquired for each sample. CDI Spec32 software (Control Development, Inc., South Bend, IN, USA) was used for the collection of Raman spectra.

The same equipment was used for in-line Raman spectroscopy measurements. The spectra were collected every 4 s for 1 h using 4 scans per spectra with a 1.0 s integration time.

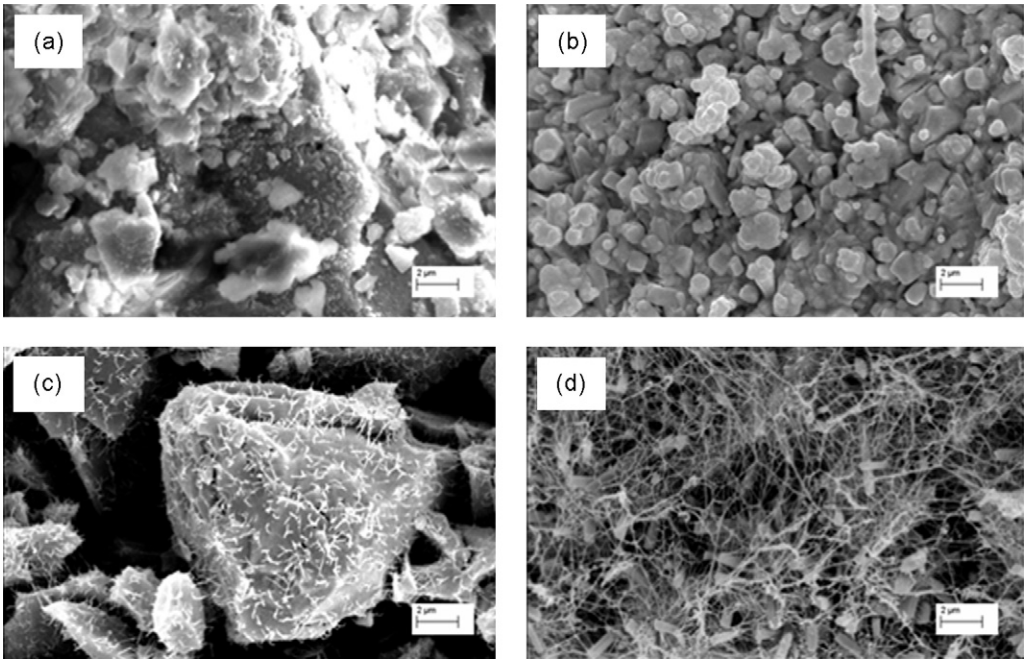

Fig. 1. SEM micrographs (5000×) of PRXAH I (a) after 180 min of milling at low temperature, and (b) after 48 h storage at 4 °C and PRXAH II (c) after 180 min of milling at low temperature and (d) after 48 h storage at 4 °C.

2.2.3. Scanning electron microscopy (SEM)

Particle size and morphology of the samples were investigated using a JSM 5200 scanning electron microscope (JEOL, Japan). Samples were mounted on aluminum stubs with double adhesive carbon tape and sputter coated with gold at 20 mA for 120 s in argon atmosphere prior to microscopy (E5200 Auto Sputter Coater, Biorad, UK).

2.2.4. Differential scanning calorimetry (DSC)

DSC was performed using a differential scanning calorimeter with refrigerated cooling system (Diamond DSC, Perkin Elmer, Waltham, MA, USA). The DSC system was calibrated for temperature and enthalpy using indium as a standard. Samples were analyzed using crimped aluminum pans and a heating rate of 10 K/min from 20 to 210 °C. Measurements were performed under nitrogen flow. Thermal events are given as onset temperatures of the events, unless mentioned otherwise.

2.2.5. Storage studies

In order to investigate the effect of temperature and time on the recrystallization behavior of amorphous PRX, the samples were stored in desiccators at ambient temperature (approx. 22 °C, RT) and at 4 °C for up to 90 h in closed glass vials over sodium silicate (silica gel). All samples were analyzed immediately after the preparation and stored under the specified storage conditions prior to further analysis.

2.2.6. Dissolution testing

The dissolution behavior of amorphous samples was investigated in simulated gastric fluid (without pepsin) (SGF) according to the USP 33 NF 28 monograph for PRX capsules. Hard gelatin capsules filled with 20 mg of the respective solid state form of PRX (mesh size 140 μm, $n = 3$) were used for dissolution testing (Erweka DT 70, Erweka GmbH, Heusenstamm, Germany). Amorphous PRX was tested immediately after preparation. A sample of 5 ml was withdrawn at 3 min interval, and replaced with an equivalent amount of dissolution medium. Detection of dissolved PRX was performed by UV spectroscopy (Evolution 300, Thermo Fisher Scientific, Waltham, MA, USA) at a wavelength of 353 nm.

Additional dissolution experiments with amorphous PRX samples as well as with crystalline PRX forms were performed with the aim to monitor the recrystallization of amorphous PRX (approx. 2 g) in a minimal amount of SGF, approx. 5 ml, by using in-line Raman spectroscopy.

Table 1
Characteristic properties of PRX forms.

Parameter	PRXAH I		PRXAH II		PRXAH III	PRXMH
Solid state	Crystalline	Amorphous	Crystalline	Amorphous	Crystalline	Crystalline
Specific peak allocations (2θ)	8.7; 11.7; 14.6; 17.8; 21.8; 27.5		9.2; 10.3; 15.9; 19.9; 20.6; 25.8		9.1; 13.1; 18.2; 25.1; 28.4; 29.5	9.6; 10.3; 12.1; 14.2; 14.7
Melting point (°C) (onset)	201.3	193.0 203.1	197.6	193.0 202.3	189	202.7
Recrystallization temperatures (°C) (onset)		50.6 87.1		66.0 100.6		
Recrystallization enthalpy (J/g)		25.2 12.6		31.1 13.3		
Solubility in SGF (mg/l)[a]	184.9		186.3		147.7	84.5

[a] Data from Vrečer et al. (2003).

2.3. Data analysis

2.3.1. Pair-wise distribution function (PDF)

Atomic pair-wise distribution function (PDF) analysis was performed by Fourier transforming the 5° to 40° 2θ region of the XRPD diffractograms using the freeware program RAD described elsewhere (Petkov, 1989). The Fourier transformation of the XRPD diffractograms is calculated according to the following equations:

$$G(r) = \frac{2}{\pi}\int_0^{Q_{max}} Q[S(Q)-1]\sin(Qr)dQ \quad (1)$$

where $G(r)$ is a probability function and r is the distance between the atoms. The structure function $S(Q)$, defined in Eq. (2), is obtained from the powder diffraction pattern which has been corrected for experimental errors and normalized and Q is the scattering vector which is defined in Eq. (3).

$$S(Q) = \frac{I^{coh}(Q) - \sum c_i \left|f_i(Q)\right|^2}{\sum c_i \left|f_i(Q)\right|^2} + 1 \quad (2)$$

where $I^{coh}(Q)$ is the measured scattering intensity that has been corrected for background and other experimental effects and c_i and f_i are the atomic concentration and X-ray atomic form factor respectively.

$$Q = \frac{4\pi \sin\theta}{\lambda} \quad (3)$$

where θ is the angle between the incident and the diffracted beam and λ is the wavelength of the beam (Egami and Billinge, 2003).

2.3.2. Multivariate data analysis (MVDA)

MVDA on PDF data was performed using principal component analysis (PCA). The PDF data were preprocessed using standard normal variate (SNV) correction and mean centering. The preprocessing, scaling and PCA on PDF data were performed using Simca-P+ software (v.12.0, Umetrics AB, Umeå, Sweden).

PCA was also used to extract and visualize the systematic variations in the XRPD and Raman spectroscopy data. The data matrix was divided into two low-dimensional matrices, scores and loadings. The diffraction range from 5° to 30° 2θ and Raman spectral region of 1000–1700 cm^{-1} was chosen for the analysis. The data were preprocessed and scaled similarly to the PDF data using SNV correction together with mean centering. All XRPD and Raman spectral data were normalized and scaled so that their relative intensity matched that of the intensity ratio in the raw diffraction patterns and spectra.

3. Results and discussion

3.1. Characterization of amorphous PRX

Chemically pure amorphous PRX (identified by the presence of only a halo in the X-ray powder diffractogram and by Raman spectroscopy) was obtained by ball-milling of PRXAH I and II at low temperature as described previously elsewhere (Kogermann et al., 2011). A different particle morphology between the amorphous samples prepared from PRXAH I and II analyzed immediately after preparation and compared to samples stored for 48 h at 4 °C was detected in the SEM images (Fig. 1a and b vs c and d). The "spider-net" like network visible between the particles (Fig. 1d) was due to crystallizing PRXAH III, as verified by XRPD and Raman spectroscopy. Characteristic properties of PRX forms are collected in Table 1.

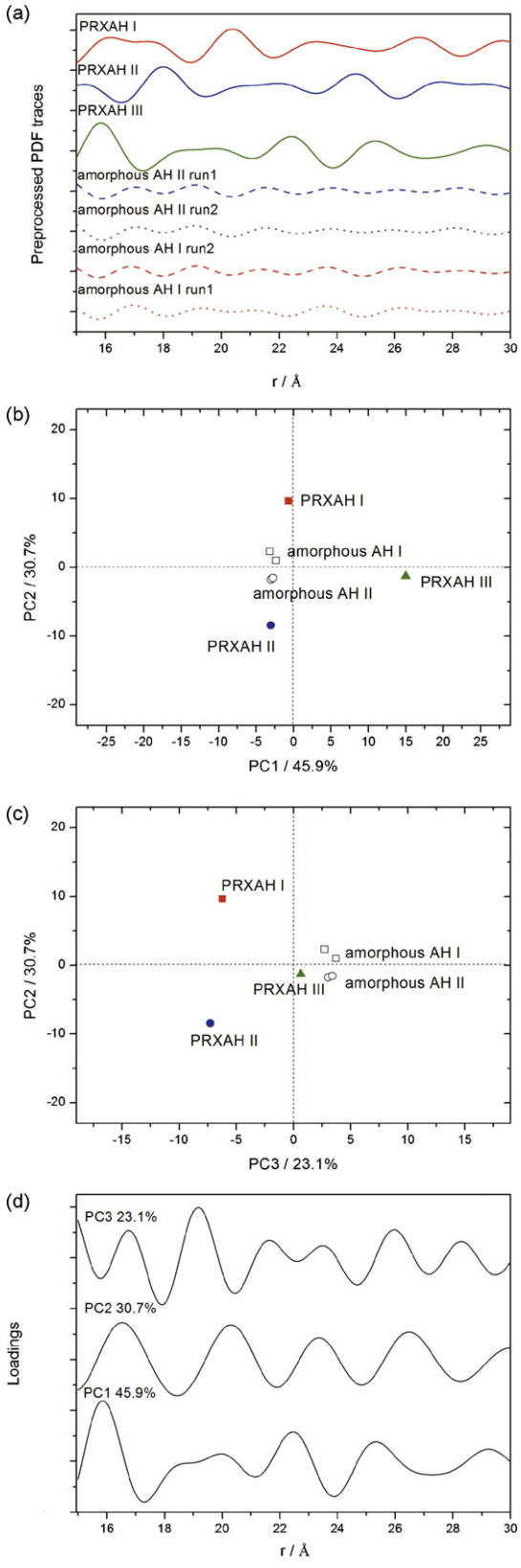

Fig. 2. (a) SNV corrected and mean centered PDF traces of untreated crystalline PRXAH I (red), PRXAH II (blue) and PRXAH III (green) (zoomed in on the interval 15–30 Å), together with X-ray amorphous PRX obtained from PRXAH I and PRXAH II by ball-milling at low temperature for 180 min, (b) PCA scores plot of PC 1 and PC 2, PRXAH I (red square), PRXAH II (blue circle), PRXAH III (green triangle) (c) PCA scores plot of PC 2 and PC 3, (d) corresponding loadings for the PC 1, PC 2 and PC 3 using PDF transformed XRPD data. (For interpretation of the references to color in this figure legend, the reader is referred to the web version of the article.)

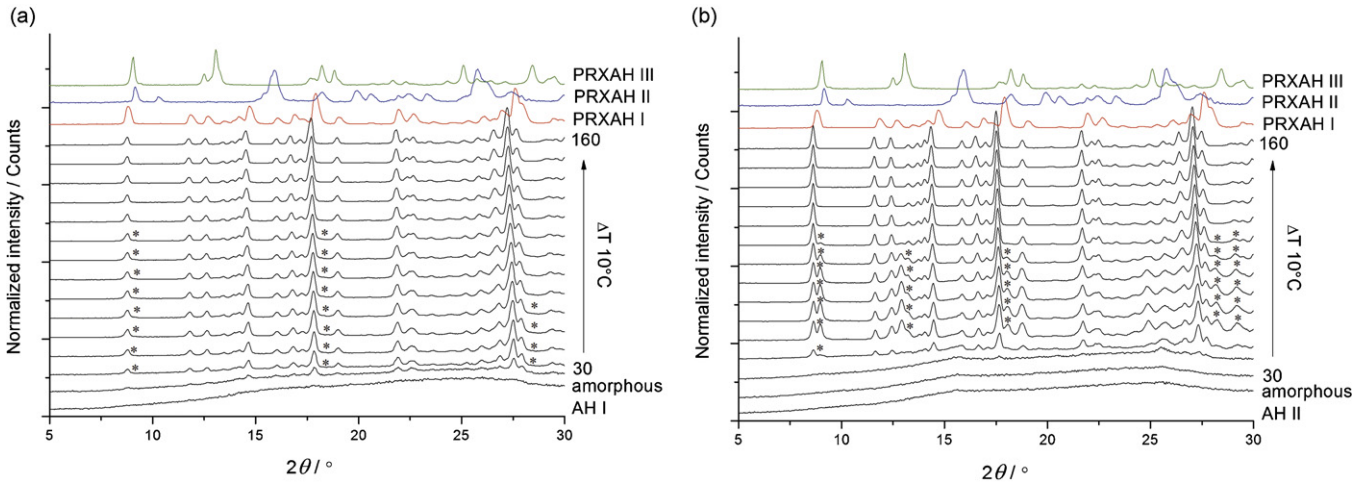

Fig. 3. VT-XRPD diffraction patterns (all patterns are normalized) of: (a) amorphous PRX prepared from PRXAH I and (b) amorphous PRX prepared from PRXAH II in comparison to XRPD patterns of untreated crystalline PRXAH forms. Heating from ambient temperature (25 °C) up to 160 °C. The (*) marks denote the reflections unique to PRXAH III.

3.2. PDF analysis of XRPD data

To investigate the differences between crystalline PRXAH I, II and III samples and amorphous samples prepared from crystalline PRXAH I and II, pair-wise distribution function (PDF) analysis was used to evaluate the X-ray diffraction data in real-space (Billinge, 2010). The three crystalline materials exhibited substantial differences in their peak positions. Furthermore, it was observed that the crystalline samples had higher peak intensities throughout the 0–30 Å interval than their amorphous counterparts. All samples, crystalline as well as amorphous, experienced a PDF trace attenuation (Fig. 2a) and this attenuation was highest for the amorphous samples. The attenuation of all the samples is in accordance with the finite Q resolution of the experiments (Eq. (3)) and amorphous samples will, due to their increased structural disorder, always exhibit a more pronounced attenuation than their crystalline counterparts (Dinnebier and Billinge, 2008). Finally, the amorphous samples prepared from PRXAH I had different peak allocations compared to the amorphous samples prepared from PRXAH II.

In order to visualize these differences between crystalline PRX samples and amorphous samples PCA was utilized. A model with three principal components (PCs) explaining 99.7% of the variation was obtained. It was observed that the first principal component (PC 1) and the second PC (PC 2) were capable of separating the three crystalline samples, i.e., PRXAH I, II and III (Fig. 2b). It was also found that PC 2 was capable of separating the amorphous samples prepared from PRXAH I from the amorphous samples prepared from PRXAH II. Furthermore, the third PC (PC 3) was capable of separating amorphous samples and PRXAH III from the crystalline samples of PRXAH I and II (Fig. 2c). In order to explain these observations it is necessary to look at the loadings of the respective PCs. The loading of PC 1 reflected the peak intensities of the preprocessed PRXAH III PDF trace (Fig. 2d). Additionally, the loading of PC 2 reflected the peak positions of the preprocessed PRXAH I PDF trace and was in antiphase to the peak positions of the preprocessed PRXAH II PDF trace (Fig. 2d). This explained the fact that the PC 2 was capable of separating the crystalline PRXAH I and II samples. Based on this argument, it is also prudent to suggest that the amorphous samples prepared from PRXAH I are closer to PRXAH I and that the amorphous samples prepared from PRXAH II are closer to PRXAH III. Finally, the loading of PC 3 was found to reflect the PDF peak intensities of the amorphous samples prepared from PRXAH I and II (Fig. 2d).

Since PC 2 did not only separate the crystalline samples but also the amorphous samples prepared from PRXAH I and II, this suggests that the starting material influenced the commonly occurring inter-atomic distances within the amorphous samples. PC 3 shows that the amorphous samples prepared from PRXAH I and II were more related to the PRXAH III samples and combining PC 2 and PC 3 indicates that the amorphous samples prepared from PRXAH II shared more common inter-atomic distances with the PRXAH III crystalline form than the amorphous samples prepared form PRXAH I did (Fig. 2c). Finally, it also prudent to mention that these tendencies found within the data set could benefit from being reexamined using a high energy radiation source e.g., a Ag anode. This would hopefully enable an even better separation of the amorphous groups.

In order to determine whether the amorphous samples prepared from PRXAH I or II have higher degree of disorder, the raw PDF traces of amorphous samples prepared from PRXAH I replicate runs were averaged and compared to the averaged amorphous samples prepared from PRXAH II replicate runs. It was observed that the averaged amorphous samples prepared from PRXAH II samples had the lowest peak intensities in 11 out of 14 peaks (79%), indicating that the amorphous samples prepared from PRXAH II possessed the highest degree of disorder.

3.3. Critical material properties

3.3.1. Impact of heat/thermal stress

In general, transformation from a less stable form to a more stable form is induced by increasing the temperature as heating increases the local mobility of the molecules. The effect of temperature on amorphous samples prepared from PRXAH I and II was investigated with VT-XRPD. Amorphous PRX prepared from PRXAH I started to crystallize as PRXAH I at 30 °C, and at 40 °C reflections with low intensity unique to PRXAH III at 9.1, 18.2 and 28.4° 2θ appeared in the X-ray diffraction pattern (Fig. 3a). Reflections belonging to PRXAH III were present until 110 °C, and at 120 °C pure PRXAH I had crystallized. Upon heating to 160 °C no other solid state changes were detected. The apparent shift in diffraction patterns as evident at Fig. 3 is due to the expansion of the crystal lattice during the non-isothermal heating (Kogermann et al., 2007a; Sheth et al., 2004a).

Amorphous samples prepared from PRXAH II showed a somewhat different thermal behavior. Crystallization started first at

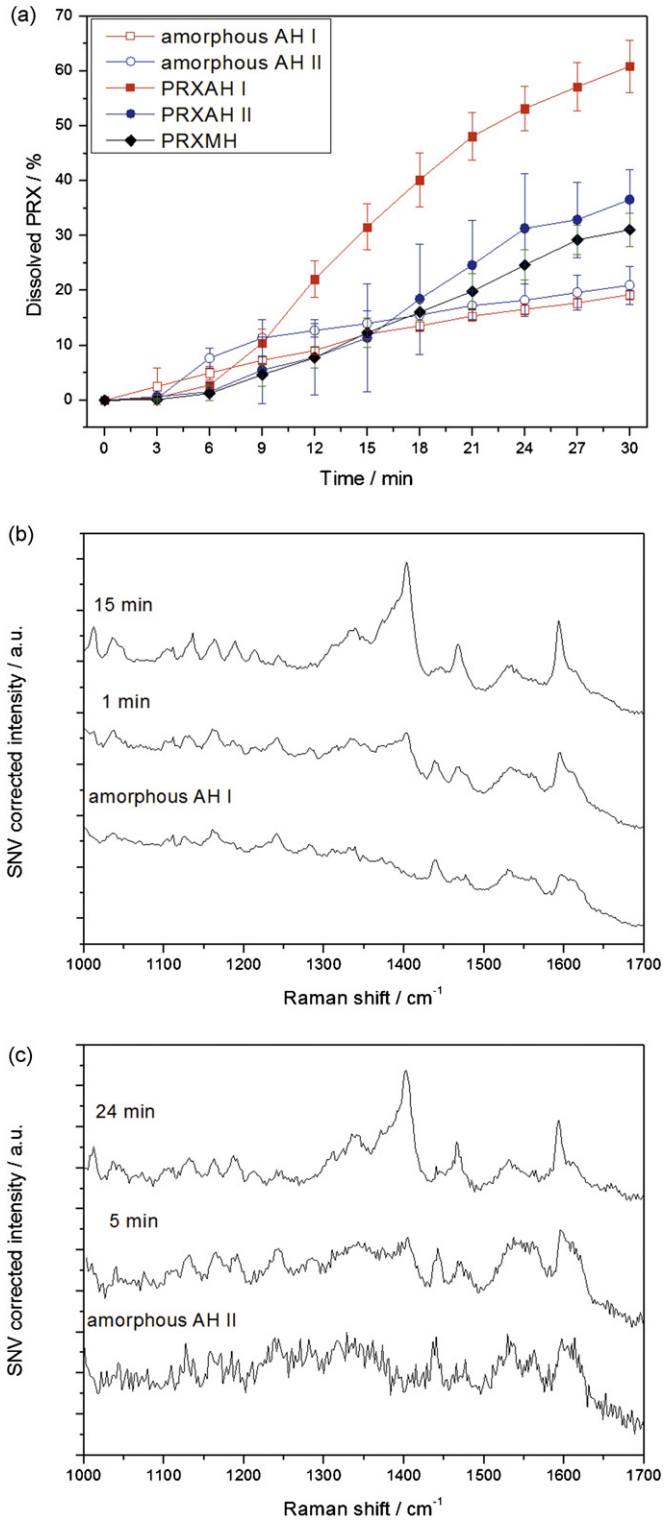

Fig. 4. (a) Dissolution profiles of amorphous PRXs and crystalline counterparts from capsules. Data expressed as mean values ± S.D. ($n = 3$); (b) amorphous PRX prepared from PRXAH I and (c) amorphous PRX prepared from PRXAH II wet slurry experiments. All experiments performed in simulated gastric fluid (SGF, pH 1.2).

50 °C where distinct reflections of PRXAH I and III appeared (Fig. 3b). Additional reflections unique to PRXAH III were seen at 13.1 and 29.5° 2θ in comparison to the amorphous samples prepared from PRXAH I, indicating the presence of higher amount of PRXAH III in samples recrystallized from amorphous samples prepared from PRXAH II. Similarly to the amorphous sample prepared from PRXAH I the PRXAH III reflections disappeared at 120 °C and only PRXAH I reflections were present up to 160 °C. The occurrence of PRXAH III may be related to the fact that the nucleation and crystal growth of the less stable form is faster compared to the more stable forms, being consistent with Ostwald's Rule of Stages.

The VT-XRPD results were supported by DSC, where two recrystallization exotherms and two melting endotherms were seen, confirming the crystallization of a mixture of two PRX forms upon non-isothermal heating. Nevertheless, the two amorphous PRX samples differed in the onset temperatures of recrystallization. Amorphous samples prepared from PRXAH I recrystallized at lower temperatures (onsets at 50.6 and 87.1 °C) together and with lower enthalpies (25.2 and 12.6 J/g) compared to amorphous samples prepared from PRXAH II (onsets at 66.0 and 100.6 °C; and enthalpies of 31.1 and 13.3 J/g). Also the melting endotherms appeared at lower temperatures for amorphous samples prepared from PRXAH I than for amorphous samples prepared from PRXAH II. None of the amorphous samples showed any evidence of a glass transition temperature (T_g) due to the temperature overlap with the recrystallization exotherms of the PRX forms. The T_g of the quench cooled samples has been reported to be at 63.9 °C for PRXAH I and 67.7 °C for PRXAH II (Kogermann et al., 2011) furthermore indicating differences between the two different amorphous samples.

The VT-XRPD and DSC results were in good agreement with the PDF analyses suggesting that amorphous samples prepared from PRXAH I were less disordered and therefore might consist some residual crystallinity. In comparison, amorphous samples prepared from PRXAH II crystallized as the less stable PRXAH III followed by further transformation to PRXAH I (as less energy is needed for recrystallization of a less stable form). The existence of seed crystals and their influence on recrystallization of amorphous samples has also been discussed by Yonemochi et al. (2005). They reported that the amorphous terfenadine prepared from form I by grinding crystallized during heating as a mixture of forms I and II, whereas ground metastable form II crystallized as pure metastable form II.

3.3.2. *Impact of dissolution medium*

Dissolution testing of amorphous materials in biorelevant media will provide important information related to the retention of the specific physicochemical properties of a drug in the amorphous state. Recrystallization of an amorphous API may occur when it comes into contact with dissolution media as recently reported by Savolainen et al. (2009) for carbamazepine. With the aim of investigating the impact of dissolution medium (SGF), and therefore obtaining further insight into the possible recrystallization behavior of amorphous PRX, dissolution studies were performed.

Dissolution studies from hard gelatin capsules in SGF were performed with both amorphous PRXs and its crystalline counterparts including PRXMH. It is relevant to state that it took approximately 3 min for the hard gelatin capsule to disintegrate. The results of the dissolution studies indicated a lower amount of PRX dissolved from both amorphous PRXs compared to the crystalline forms during 30 min of testing (Fig. 4a). However, the advantage of a higher apparent solubility of amorphous material was still present in the early phase of dissolution testing (<10 min) for both amorphous PRXs as the percentage of PRX dissolved was higher compared to the percentage of PRX dissolved from crystalline forms. The percentage of PRX dissolved from both amorphous materials was similar after the early phase (>10 min) in SGF. The sudden drop in the dissolution rate of amorphous PRXs indicated a possible fast recrystallization of amorphous material in the presence of SGF.

In order to further investigate the recrystallization behavior of amorphous PRXs in SGF in-line Raman spectroscopy was used to

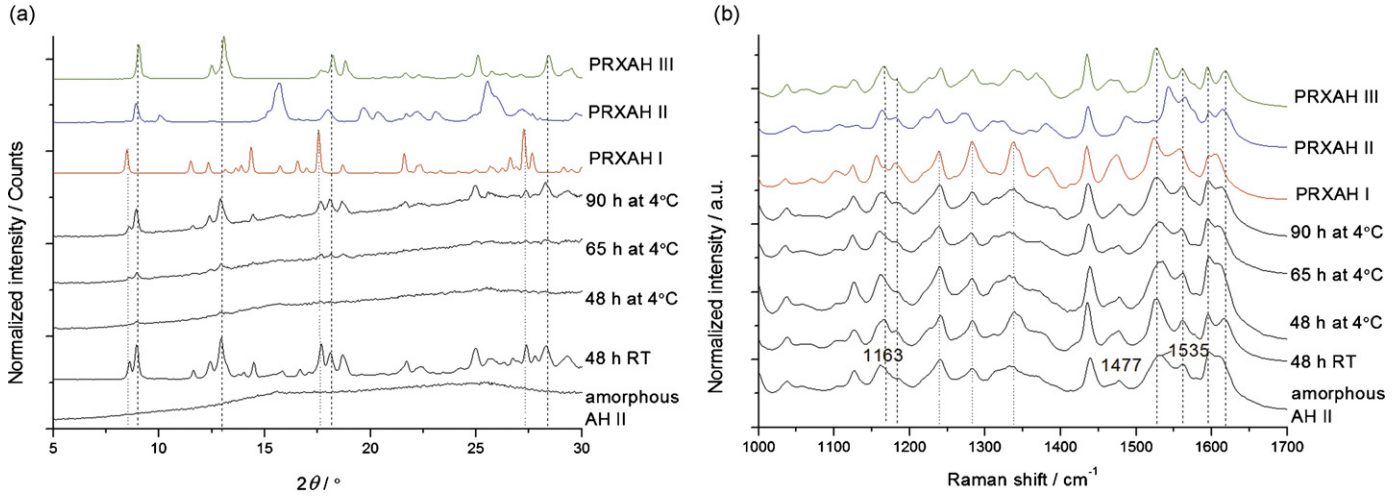

Fig. 5. (a) XRPD patterns and (b) Raman spectra of untreated crystalline PRXAH I (red), PRXAH II (blue), PRXAH III (green) and obtained amorphous samples after 180 min milling of PRXAH II at low temperature, and samples stored at ambient temperature (RT) and at 4 °C over silica gel. Time points of measurements during storage: 48, 65 and 90 h after preparation, for clarification the RT sample patters shown only after 48 h of storage as no further changes in Raman spectra were detected after 65 and 90 h of storage. XRPD reflections and Raman peaks of PRXAH I and PRXAH III are denoted with dotted line (···) and dashed line (- - -), respectively. (For interpretation of the references to color in this figure legend, the reader is referred to the web version of the article.)

monitor the phase transformations in the presence of a minimal amount of dissolution medium. Differences in the recrystallization behavior of the two amorphous PRXs could be identified. Again, amorphous samples obtained from PRXAH I showed faster recrystallization, already during the first minute of dissolution testing in SGF (Fig. 4b), whereas amorphous samples prepared from PRXAH II showed first signs of PRXMH recrystallization after 5 min (Fig. 4c). PRXMH exhibits the lowest intrinsic dissolution rate compared to other crystalline PRX forms (Vrečer et al., 2003) explaining the decline in the dissolution rate of amorphous PRXs. The crystalline PRX forms did not show any SGF induced solid state changes in the tested time interval. The solid state changes of amorphous material in SGF were also confirmed by XRPD (data not shown). It was shown with the dissolution testing that the expected advantage of faster dissolution and higher bioavailability of amorphous material was actually lost in the case of amorphous PRX.

3.3.3. *Impact of storage*

The physical stability of amorphous material during storage is another important factor regarding the final product performance. Therefore the influence of storage time and temperature on the recrystallization behavior of the amorphous forms of PRX was investigated. Amorphous PRX samples were physically very unstable and started to crystallize immediately after preparation. However, the time-scale of solid state changes still differed between the two amorphous samples. The XRPD results revealed that amorphous PRX, obtained from PRXAH I, crystallized as almost pure PRXAH I after 48 h of storage over silica gel in closed vials at RT and at 4 °C. The amorphous samples stored at RT exhibited diffractions of PRXAH III, but these were hardly detectable. After longer storage times (up to 90 h) crystallization of amorphous material continued, as detected by the increased reflection intensities, however no additional phase transformations could be identified. Raman spectroscopy confirmed the observations made with XRPD. Samples measured after 48 h of storage at RT showed mainly PRXAH I peaks, and only minor peaks indicating the possible presence of PRXAH III were identified. Raman spectra exhibited a higher amount of amorphous PRX in samples stored at 4 °C for 48 h. Upon further storage, only a change in intensity was detected due to increased crystallinity of the samples.

According to the XRPD and Raman data, the amorphous PRX obtained from PRXAH II had recrystallized into a mixture of PRXAH I and III during storage for 48 h at RT (Fig. 5a and b). For the samples stored at 4 °C for 48 h a very weak reflection belonging to PRXAH III had appeared at 9.1° 2θ in the XRPD pattern (Fig. 5a). After 65 h of storage the samples had crystallized as a mixture of PRXAH I and III, with an even higher crystallinity after 90 h (Fig. 5a). XRPD results were again confirmed by Raman spectroscopy, with peaks belonging to PRXAH I and III detectable in the samples stored for 48 h at RT (Fig. 5b). Interpretation of the Raman spectra for samples stored at 4 °C was more difficult as the presence of several solid forms was identified. In order to deal efficiently with the interpretation of the results MVDA tools were therefore applied.

3.3.4. *MVDA for identification of complex recrystallization pathways*

MVDA has become a well recognized approach for interpretation and identification of complex phenomena. PCA is one possible MVDA tool that has been used to investigate and visualize the solid state changes (Jørgensen et al., 2006). In this study PCA was carried out for several datasets with the aim to investigate the effect of storage time and temperature on the two amorphous PRX samples (Fig. 6). Three PCs were used to describe the variation in XRPD and Raman spectral data, respectively. PCA scores and loading vector of the PC 1 explained 41.4% of the variation in the XRPD data, separating crystalline, amorphous and recrystallized samples (Fig. 6a). The PC 2 and PC 3 explained 26.3% and 19.3% of the variation, respectively. Interestingly, the loading vector of PC 2 represented reflections of PRXAH III and amorphous halo, and therefore separated PRXAH III from all other samples (Fig. 6c and e). The PC 3 separated PRXAH II from other samples. PCA also confirmed that independent of the storage conditions, samples prepared from PRXAH I were more crystalline after the same storage time than samples prepared from PRXAH II (Fig. 6a). It is also evident from the scores plot (Fig. 6a) that amorphous samples prepared from PRXAH I stored at RT had crystallized as almost pure PRXAH I, and amorphous samples prepared from PRXAH II as a mixture of PRXAH I and III.

The largest variation in Raman spectral data was explained by the scores and loading vector for PC 1 (53.4%), separating amorphous PRX forms from crystalline ones (Fig. 6b and d). In addition, the PC 2 (19.3%) differentiated PRXAH I and II amorphous samples from crystalline ones. The PC 3 (14.6%) separated PRX crystalline forms from each other. In general, the PCA models of

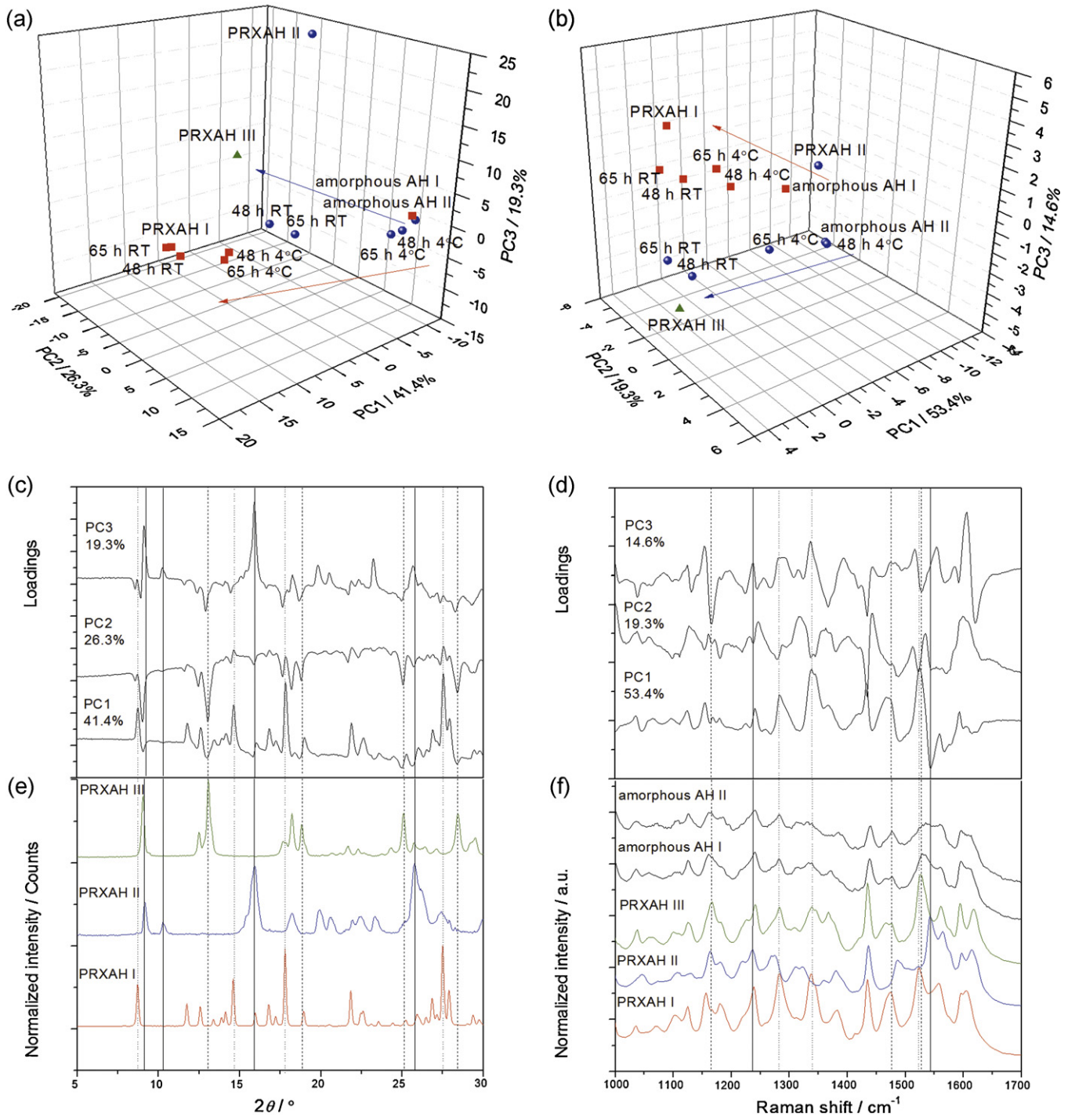

Fig. 6. Principal component analysis (PCA) plots of piroxicam (PRX) forms during storage at room temperature (RT) and at 4 °C together with untreated crystalline PRXAH I (red squares), PRXAH II (blue circles), PRXAH III (green triangle). (a) XRPD PCA 3D scores plot for the PC 1, PC 2 and PC 3; (c) loadings for the PCs; (e) XRPD patterns of untreated PRXAH forms; (b) Raman spectroscopy PCA 3D scores plot for the PC 1, PC 2 and PC 3; (d) loadings for the PCs; (f) Raman spectra of untreated PRXAH forms and amorphous material. Arrows point out the movement; numbers represent the sampling time points (min). Dotted (···), solid (—), and dashed (- - -) lines represent the reflections unique to PRXAH I, PRXAH II, and PRXAH III, respectively. All patterns are normalized. (For interpretation of the references to color in this figure legend, the reader is referred to the web version of the article.)

Raman spectral data showed similar results and the same trends as the XRPD data (Fig. 6a and b). However, additional information was obtained emphasizing the complementary characteristics of XRPD and Raman spectroscopy. For example, PRXAH I amorphous sample stored for 48 h at RT was detected as almost pure crystalline PRXAH I in the XRPD PCA model. Albeit, the PCA model of Raman data indicated movement closer to starting crystalline PRXAH I but it still differed from the untreated crystalline material. The small differences between the different crystalline forms are less significant in the XRPD PCs than in the Raman PCs, as the amorphous form has a characteristic halo in XRPD pattern which differs greatly from the diffraction pattern of crystalline samples, getting higher values in PC scores and loadings compared to a peak shift or intensity change in Raman spectra.

4. Conclusions

The critical material characteristics (e.g., amorphous state) need to be thoroughly investigated especially with regard to stability and product performance. The recrystallization of amorphous PRX samples depended on the starting solid state form, PRXAH I vs II. The lower physical stability of amorphous PRX prepared from PRXAH I compared to amorphous PRX prepared from PRXAH II is linked to the higher residual order in amorphous samples obtained from PRXAH I as was also identified by PDF analysis. According to the recrystallization behavior of the amorphous samples prepared from PRXAH I they were closely related to the starting material, whereas the recrystallization behavior of amorphous samples prepared from PRXAH II resembled to that of the PRXAH III. MVDA approach had to be used in order to fully understand the impact of storage time and temperature on amorphous state. According to the MVDA the influence of storage time and temperature was more pronounced in case of amorphous PRX prepared from PRXAH I than from PRXAH II, indicating the possible presence of higher residual order in X-ray amorphous PRXAH I samples.

The performed dissolution experiments confirmed that the amorphous PRX obtained from PRXAH II recrystallized slower as PRXMH in biorelevant dissolution medium compared to amorphous PRX obtained from PRXAH I. However, this study also indicates that the advantage of faster dissolution of amorphous material was actually lost and a lower dissolution of amorphous material compared to the initial crystalline materials was obtained.

Acknowledgments

This work is part of grant project no. ETF7980 and the targeted financing project no. SF0180042s09 financed by The Estonian Science Foundation and the Estonian Minister of Education and Research. The authors are grateful to Prof Dr. Franc Vrečer (Krka, d.d., R&D Division, Slovenia) for providing XRPD and Raman spectral data of PRXAH III for comparison. The grant from Lundbeckfonden (Copenhagen, Denmark) for the purchase of the X-ray powder diffractometer is greatly acknowledged (grant decision 479/06). The Danish Agency for Science, Technology and Innovation is acknowledged for financial support through the Innovation Consortium NanoMorph project (grant decision 952320). Dorthe Kyed Ørbæk (University of Copenhagen) is recognized for SEM measurements and Dr. Mingshi Yang (University of Copenhagen) for help with the spray drier.

References

Allen, F.H., 2002. The Cambridge Structural Database: a quarter of a million crystal structures and rising. Acta Crystallogr. B 58, 380–388.

Aso, Y., Yoshioka, S., Kojima, S., 2003. Molecular mobility-based estimation of the crystallization rates of amorphous nifedipine and phenobarbital in poly(vinylpyrrolidone) solid dispersions. J. Pharm. Sci. 93, 384–391.

Augustijns, P., Brewster, M.E., 2012. Supersaturating drug delivery systems: fast is not necessarily good enough. J. Pharm. Sci. 101, 7–9.

Bates, S., Zografi, G., Engers, D., Morris, K., Crowley, K., Newman, A., 2006. Analysis of amorphous and nanocrystalline solids from their X-ray diffraction patterns. Pharm. Res. 23, 2333–2349.

Billinge, S.J.L., 2010. Characterisation of amorphous and nanocrystalline molecular materials by total scattering. CrystEngComm 12, 1366–1368.

Bordner, J., Richards, J.A., Weeks, P., Whipple, E.B., 1984. Piroxicam monohydrate: a zwitterionic form, $C_{15}H_{13}N_3O_4S{\cdot}H_2O$. Acta Crystallogr. C 40, 989–990.

Boetker, J.P., Karmwar, P., Strachan, C.J., Cornett, C., Tian, F., Zujovic, Z., Rantanen, J., Rades, T., 2011. Assessment of crystalline disorder in cryo-milled samples of indomethacin using atomic pair-wise distribution functions. Int. J. Pharm. 417, 112–119.

Brouwers, J., Brewster, M.E., Augustijns, P., 2009. Supersaturating drug delivery systems: the answer to solubility-limited oral bioavailability? J. Pharm. Sci. 98, 2549–2572.

Craig, D.Q.M., Barsnes, M., Royall, P.G., Kett, V.L., 2000. An evaluation of the use of modulated temperature DSC as a means of assessing the relaxation behaviour of amorphous lactose. Pharm. Res. 17, 696–700.

Crowley, K.J., Zografi, G., 2002. Cryogenic grinding of indomethacin polymorphs and solvates: assessment of amorphous phase formation and amorphous phase physical stability. J. Pharm. Sci. 91, 492–507.

Dinnebier, R.E., Billinge, S.J.L., 2008. Powder Diffraction: Theory and Practice. Royal Society of Chemistry, Cambridge.

Egami, T., Billinge, S.J.L., 2003. Underneath the Bragg peaks: structural analysis of complex materials. In: Cahn, R.W. (Ed.), Pergamon Materials Series. Pergamon Press, Elsevier Ltd., Oxford.

Graeser, K.A., Patterson, J.E., Zeitler, J.A., Gordon, K.C., Rades, T., 2009. Correlating thermodynamic and kinetic parameters with amorphous stability. Eur. J. Pharm. Sci. 37, 492–498.

Hilden, L.R., Morris, K.R., 2003. Prediction of the relaxation behavior of amorphous pharmaceutical compounds. I: master curves concept and practice. J. Pharm. Sci. 92, 1464–1472.

ICH, 2009. ICH Q8(R2) Guidance for Industry. Pharmaceutical Development, International Conference on Harmonization EMEA/CHMP/ICH/167068/042006.

Ingkatawornwong, S., Kaewnopparat, N., Tantishaiyakul, V., 2001. Studies on aging piroxicam–polyvinylpyrrolidone solid dispersions. Pharmazie 56, 227–230.

Jinno, J., Oh, D.M., Crison, J.R., Amidon, G.L., 2000. Dissolution of ionizable water-insoluble drugs: the combined effect of pH and surfactant. J. Pharm. Sci. 89, 268–274.

Jørgensen, A.C., Miroshnyk, I., Karjalainen, M., Jouppila, K., Siiriä, S., Antikainen, O., Rantanen, J., 2006. Multivariate data analysis as a fast tool in evaluation of solid state phenomena. J. Pharm. Sci. 95, 906–916.

Karmwar, P., Boetker, J., Graeser, K., Strachan, C.J., Rantanen, J., Rades, T., 2011a. Investigations on the effect of different cooling rates on the stability of amorphous indomethacin. Eur. J. Pharm. Sci. 44, 341–350.

Karmwar, P., Graeser, K., Gordon, K.C., Strachan, C.J., Rades, T., 2011b. Investigation of properties and recrystallisation behaviour of amorphous indomethacin samples prepared by different methods. Int. J. Pharm. 417, 94–100.

Kogermann, K., Aaltonen, J., Strachan, C.J., Pöllänen, K., Heinämäki, J., Yliruusi, J., Rantanen, J., 2008. Establishing quantitative in-line analysis of multiple solid-state transformations during dehydration. J. Pharm. Sci. 97, 4983–4999.

Kogermann, K., Aaltonen, J., Strachan, C.J., Pöllänen, K., Veski, P., Heinämäki, J., Yliruusi, J., Rantanen, J., 2007a. Qualitative in situ analysis of multiple solid-state forms using spectroscopy and partial least squares discriminant modeling. J. Pharm. Sci. 96, 1802–1820.

Kogermann, K., Zeitler, J.A., Rantanen, J., Rades, T., Taday, P.F., Pepper, M., Heinämäki, J., Strachan, C.J., 2007b. Investigating dehydration from compacts using terahertz pulsed Raman and near-infrared spectroscopy. Appl. Spectrosc. 61, 1265–1274.

Kogermann, K., Veski, P., Rantanen, J., Naelapää, K., 2011. X-ray powder diffractometry in combination with principal component analysis – a tool for monitoring solid state changes. Eur. J. Pharm. Sci. 43, 278–289.

Kojic-Prodic, B., Ruzic-Toros, Z., 1982. Structure of piroxicam. Acta Crystallogr. B 38, 2948.

Morris, K.R., Griesser, U.J., Eckhardt, C.J., Stowell, J.G., 2001. Theoretical approaches to physical transformations of active pharmaceutical ingredients during manufacturing processes. Adv. Drug Deliv. Rev. 48, 91–114.

Petkov, V., 1989. Simultaneity, conventionality and existence. Br. J. Philos. Sci. 40, 69–76.

Reck, G., Dietz, G., Laban, G., Günther, W., Bannier, G., Höhne, E., 1988. X-ray studies on piroxicam modifications. Pharmazie 43, 477–481.

Savolainen, M., Heinz, A., Strachan, C.J., Gordon, K.C., Yliruusi, J., Rades, T., Sandler, N., 2007. Screening for differences in the amorphous state of indomethacin using multivariate visualization. Eur. J. Pharm. Sci. 30, 113–123.

Savolainen, M., Kogermann, K., Heinz, A., Aaltonen, J., Peltonen, L., Strachan, C., Yliruusi, J., 2009. Better understanding of dissolution behaviour of amorphous drugs by in situ solid-state analysis using Raman spectroscopy. Eur. J. Pharm. Biopharm. 71, 71–79.

Shakhtshneider, T.P., Danéde, F., Capet, F., Willart, J.F., Descamps, M., Myz, S.A., Boldyreva, E.V., Boldyrev, V.V., 2007. Grinding of drugs with pharmaceutical excipients at cryogenic temperatures. Part I: cryogenic grinding of piroxicam–polyvinylpyrrolidone mixtures. J. Therm. Anal. Calorim. 89, 699–707.

Sheth, A.R., Bates, S., Muller, F.X., Grant, D.J.W., 2004a. Local structure in amorphous phases of piroxicam from powder X-ray diffractometry. Cryst. Growth Des. 5, 571–578.

Sheth, A.R., Bates, S., Muller, F.X., Grant, D.J.W., 2004b. Polymorphism in piroxicam. Cryst. Growth Des. 4, 1091–1098.

Shibata, Y., Fujii, M., Kokudai, M., Noda, S., Okada, H., Kondoh, M., Watanabe, Y., 2006. Effect of characteristics of compounds on maintainance of an amorphous state in solid dispersion with crospovidone. J. Pharm. Sci. 96, 1537–1547.

Surana, R., Pyne, A., Suryanarayanan, R., 2004a. Effect of aging on the physical properties of amorphous trehalose. Pharm. Res. 21, 867–874.

Surana, R., Pyne, A., Suryanarayanan, R., 2004b. Effect of preparation method on physical properties of amorphous trehalose. Pharm. Res. 21, 1167–1176.

Vrečer, F., Vrbinc, M., Meden, A., 2003. Characterization of piroxicam crystal modifications. Int. J. Pharm. 256, 3–15.

Winkel, K., Hage, W., Loerting, T., Price, S.L., Mayer, E., 2007. Carbonic acid: from polyamorphism to polymorphism. J. Am. Chem. Soc. 129, 13863–13871.

Yonemochi, E., Hoshino, T., Yoshihashi, Y., Terada, K., 2005. Evaluation of the physical stability and local crystallization of amorphous terfenadine using XRD–DSC and micro-TA. Thermochim. Acta 432, 70–75.